Wireless Personal Communications **13:** 119–143, 2000.

Adaptive Modulation over Nakagami Fading Channels *

MOHAMED-SLIM ALOUINI**
Communications Group, Department of Electrical Engineering, California Institute of Technology (Caltech), Pasadena, CA, U.S.A.

ANDREA J. GOLDSMITH
Department of Electrical Engineering, Mail Code 9515, Stanford University, Stanford, CA 94305-9515, U.S.A.
E-mail: andrea@ee.stanford.edu

Abstract. We first study the capacity of Nakagami multipath fading (NMF) channels with an average power constraint for three power and rate adaptation policies. We obtain closed-form solutions for NMF channel capacity for each power and rate adaptation strategy. Results show that rate adaptation is the key to increasing link spectral efficiency. We then analyze the performance of practical constant-power variable-rate M-QAM schemes over NMF channels. We obtain closed-form expressions for the outage probability, spectral efficiency and average bit-error-rate (BER) assuming perfect channel estimation and negligible time delay between channel estimation and signal set adaptation. We also analyze the impact of time delay on the BER of adaptive M-QAM.

Keywords: link spectral efficiency, adaptive modulation techniques, and Nakagami fading.

1. Introduction

The radio spectrum available for wireless services is extremely scarce, while demand for these services is growing at a rapid pace [1]. Hence spectral efficiency is of primary concern in the design of future wireless data communications systems. In this paper we first investigate the theoretical spectral efficiency limits of adaptive transmission in Nakagami multipath fading (NMF) channels [2]. We then propose and study adaptive multi-level quadrature amplitude modulation (M-QAM) schemes which improve link spectral efficiency (R/W [bits/sec/Hz]), defined as the average transmitted data rate per unit bandwidth for a specified average transmit power and bit-error-rate (BER). We also evaluate the performance of these schemes relative to the theoretical spectral efficiency limit.

Mobile radio links can exhibit severe multipath fading which leads to serious degradation in the link carrier-to-noise ratio (CNR) and consequently a higher BER. Fading compensation such as an increased link budget margin or interleaving with channel coding are typically required to improve link performance. However, these techniques are designed relative to the worst-case channel conditions, resulting in poor utilization of the full channel capacity a good percentage of the time (i.e., under negligible or shallow fading conditions). Adapting certain

* This work was supported in part by a National Semiconductor (NSC) Graduate Fellowship Award and in part by the Office of Naval Research (ONR) under Grant No. NAV-5X-N149510861. This is an expanded version of work which was presented at the 1997 *IEEE Vehicular Technology Conference* (VTC'97), Phoenix, Arizona, U.S.A., May 1997 and the 6th Communication Theory Mini-Conference (CTMC-VI) in conjunction with *IEEE Global Communications Conference* (GLOBECOM'97), Phoenix, Arizona, U.S.A., November 1997.

** Now with the Department of electrical and Computer Engineering, University of Minnesota, 200 Union Street S.E., Minneapolis, MN 55455, U.S.A. E-mail: alouini@ece.umn.edu

parameters of the transmitted signal to the channel fading leads to better utilization of the channel capacity. The basic concept of adaptive transmission is real-time balancing of the link budget through adaptive variation of the transmitted power level, symbol transmission rate, constellation size, coding rate/scheme, or any combination of these parameters [3–7]. Thus, without wasting power or sacrificing BER, these schemes provide a higher average link spectral efficiency by taking advantage of the time-varying nature of wireless channels: transmitting at high speeds under favorable channel conditions and responding to channel degradation through a smooth reduction of their data throughput. Good performance of these schemes requires accurate channel estimation at the receiver and a reliable feedback path between that estimator and the transmitter. Furthermore since outage probability of such schemes can be quite high, especially for channels with low average CNR, adaptive systems may require buffering of the input data.

The Shannon capacity of a channel defines its maximum possible rate of data transmission for an arbitrarily small BER, without any delay or complexity constraints. Therefore the Shannon capacity represents an upper bound for practical communication schemes, and also serves as a bench-mark against which to compare the spectral efficiency of adaptive transmission schemes [8]. In [9] the capacity of a single-user flat-fading channel with perfect channel measurement information at the transmitter and receiver was derived for various adaptive transmission policies. In this paper we apply the general theory developed in [9] to obtain closed-form expressions for the capacity of NMF channels under different adaptive transmission schemes. In particular, we consider three adaptive policies: optimal simultaneous power and rate adaptation, constant power with optimal rate adaptation, and channel inversion with fixed rate. We then present numerical results showing that rate adaptation is the key to achieving high link spectral efficiency. Rate adaptation can be achieved through a variation of the symbol time duration [3] or constellation size [5]. The former method requires complicated hardware and results in a variable-bandwidth system without additional spectral efficiency, whereas the latter technique is better suited for hardware implementation, and results in a spectrally efficient variable-throughput system with a fixed bandwidth. Based on these advantages we analyze the performance of constant-power variable-rate M-QAM schemes for spectrally efficient data transmission over NMF channels. Similar analysis has been presented in [6] for a variable-power variable-rate M-QAM in Rayleigh fading and log-normal shadowing, and in [10] for constant-power variable-rate M-QAM in Rayleigh fading. We extend the results of [6, 10] to constant-power variable-rate M-QAM by analyzing the resulting spectral efficiency and BER for the more general NMF distribution. We also analyze the impact of time delay on the performance of adaptive M-QAM.

The remainder of this paper is organized as follows. In Section 2 we outline the channel and communication system models. In Section 3 we derive the capacity of NMF channels for the optimal adaptive policy, constant power policy, and channel inversion policy, and we present some numerical examples comparing (i) the NMF channel capacity with the capacity of an additive white Gaussian noise (AWGN) channel, and (ii) the NMF channel capacity for the various adaptive policies. In Section 4 we propose and evaluate the performance of a practical adaptive constant-power variable-rate M-QAM system assuming perfect channel estimation and negligible time delay between channel estimation and signal set adaptation. The BER degradation due to time delay is analyzed in Section 5. A summary of our results is presented in Section 6.

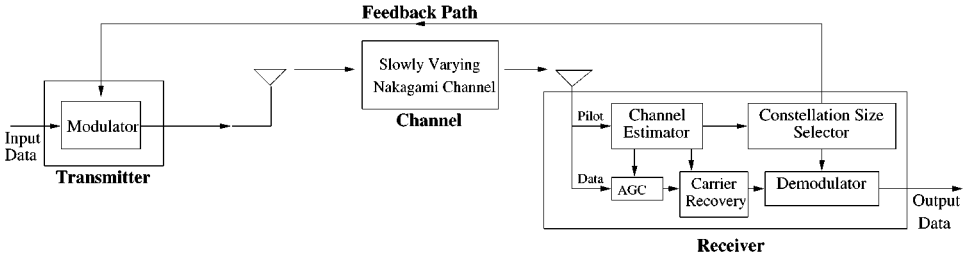

Figure 1. Adaptive communication system model.

2. System and Channel Models

2.1. Adaptive Communication System Model

A block diagram of the adaptive communication system is shown in Figure 1. A pilot tone continually sends a known "channel sounding" sequence so that the channel-induced envelope fluctuation α and phase shift ϕ can be extracted at the channel estimation stage. Based on this channel gain estimate $\hat{\alpha}$, a decision device selects the rate and power to be transmitted, configures the demodulator accordingly, and informs the transmitter about that decision via the feedback path. The constellation size assignment for the proposed constant-power variable-rate M-QAM scheme will be discussed in more detail in Section 4.1. The transmission system keeps its configuration unchanged (i.e., no re-adaptation) for a duration τ_t [s]. Meanwhile, the phase estimate $\hat{\phi}$ is used at the receiver for full compensation of the phase variation (i.e., ideal coherent phase detection), whereas the channel gain estimate $\hat{\alpha}$ is used on a continuous basis by the automatic gain controller (AGC)/demodulator for symbol-by-symbol maximum-likelihood detection.

For satisfactory operation the modulator and demodulator must be configurated at any instant for the same constellation size. Efficient error control schemes are therefore required to insure an error-free feedback path. However, such schemes inevitably introduce a certain time delay τ_{fb} [s], which may include decoding/ARQ delay, and propagation time via the feedback path. Hence, even if perfect channel estimates are available at the receiver, the system will not be able to adapt to the actual channel fading but rather to at best a τ_{fb} delayed version of it. In practice, the choice of the power and/or constellation is based on a channel estimate at time t, but the data are sent over the channel at time $t + \tau$ such that $\tau_{fb} \leq \tau \leq \tau_t$, where $1/\tau_t$ is the rate at which we change the constellation size and power. The goal is to operate with the smallest possible τ_{fb} to minimize the impact of feedback delay, and with the largest possible τ_t to minimize the rate of system reconfiguration. This issue will be further discussed in Section 5.

2.2. Channel Model and Fading Statistics

We consider a slowly-varying flat-fading channel changing at a rate much slower than the symbol data rate, so the channel remains roughly constant over hundreds of symbols. The multipath fading environment can be characterized by different statistical models. For NMF channels the probability distribution function (PDF) of the channel gain α is given by [2, (11)]

$$p_\alpha(\alpha) = 2\left(\frac{m}{\Omega}\right)^m \frac{\alpha^{2m-1}}{\Gamma(m)} \exp\left(-m\frac{\alpha^2}{\Omega}\right), \qquad \alpha \geq 0, \tag{1}$$

where $\Omega = E(\alpha^2)$ is the average fading power, m is the Nakagami fading parameter ($m \geq 1/2$), and $\Gamma(.)$ is the gamma function [11]. The received CNR, γ, is then gamma distributed according to the PDF, $p_\gamma(\gamma)$, given by

$$p_\gamma(\gamma) = \left(\frac{m}{\overline{\gamma}}\right)^m \frac{\gamma^{m-1}}{\Gamma(m)} \exp\left(-m\,\frac{\gamma}{\overline{\gamma}}\right), \qquad \gamma \geq 0, \tag{2}$$

where $\overline{\gamma}$ is the average received CNR. The phase ϕ of the Nakagami fading is uniformly distributed over $[0,2\pi]$.

The Nakagami fading represents a wide range of multipath channels via the *m fading parameter* [2]. For instance, the Nakagami-*m* distribution includes the one-sided Gaussian distribution ($m = 1/2$, which corresponds to the highest amount of multipath fading scenario) and the Rayleigh distribution ($m = 1$) as special cases. In addition, when $m > 1$, a one-to-one mapping between the Rician factor and the Nakagami fading parameter allows the Nakagami-*m* distribution to closely approximate the Rice distribution [2]. Finally, and perhaps most importantly, the Nakagami-*m* distribution often gives the best fit to urban [12] and indoor [13] multipath propagation.

3. Capacity of Nakagami Fading Channels

In this section we present closed-form expressions for the capacity of NMF channels under various power and rate adaptation policies and assuming perfect channel estimation (i.e., $\hat{\gamma} = \gamma$) and negligible time delay between channel estimation and signal set adaptation ($\tau = 0$).

3.1. Optimal Adaptation

Given an average transmit power constraint, the channel capacity of a fading channel with received CNR distribution $p_\gamma(\gamma)$ and optimal power and rate adaptation ($< C >_{\text{opra}}$ [bit/sec]) is given in [9] as

$$< C >_{\text{opra}} = W \int_{\gamma_o}^{+\infty} \log_2\left(\frac{\gamma}{\gamma_o}\right)\, p_\gamma(\gamma)\, d\gamma, \tag{3}$$

where W [Hz] is the channel bandwidth and γ_o is the optimal cutoff CNR level below which data transmission is suspended. This optimal cutoff must satisfy the equation

$$\int_{\gamma_o}^{+\infty} \left(\frac{1}{\gamma_o} - \frac{1}{\gamma}\right)\, p_\gamma(\gamma)\, d\gamma \;= 1. \tag{4}$$

To achieve the capacity (3), the channel fade level must be tracked at both the receiver and transmitter, and the transmitter has to adapt its power and rate accordingly, allocating high power levels and rates for good channel conditions (γ large), and lower power levels and rates for unfavorable channel conditions (γ small). Since no data is sent when $\gamma < \gamma_o$, the optimal policy suffers a probability of outage P_{out}, equal to the probability of no transmission, given by

$$P_{\text{out}} = \int_0^{\gamma_o} p_\gamma(\gamma)\, d\gamma = 1 - \int_{\gamma_o}^{+\infty} p_\gamma(\gamma)\, d\gamma. \tag{5}$$

Substituting (2) in (4) we find that γ_o must satisfy

$$\frac{\Gamma\left(m, m\,\frac{\gamma_o}{\overline{\gamma}}\right)}{\frac{\gamma_o}{\overline{\gamma}}} - m\,\Gamma\left(m-1, m\,\frac{\gamma_o}{\overline{\gamma}}\right) = \overline{\gamma}\,\Gamma(m), \tag{6}$$

where $\Gamma(.,.)$ is the complementary incomplete gamma function [11]. For the special case of the Rayleigh fading channel ($m = 1$), (6) reduces to

$$\frac{e^{-\gamma_o/\overline{\gamma}}}{\gamma_o/\overline{\gamma}} - E_1\left(\frac{\gamma_o}{\overline{\gamma}}\right) = \overline{\gamma}, \tag{7}$$

where $E_1(\cdot)$ is the exponential integral of first order defined by

$$E_1(x) = \int_1^{\infty} \frac{e^{-xt}}{t}\,dt; \qquad x \geq 0.$$

Let $x = \gamma_o/\bar{\gamma}$ and define

$$f(x) = \frac{\Gamma(m, m\,x)}{x} - m\,\Gamma(m-1, m\,x) - \overline{\gamma}\,\Gamma(m). \tag{8}$$

Note that $\frac{df(x)}{dx} = \frac{-\Gamma(m,mx)}{x^2} < 0$ for all $x \geq 0$. Moreover, from (8), $\lim_{x\to 0^+} f(x) = +\infty$ and $\lim_{x\to+\infty} f(x) = -\overline{\gamma}\,\Gamma(m) < 0$. Thus there is a unique positive x_o for which $f(x_o) = 0$ or, equivalently, there is a unique γ_o which satisfies (6). An asymptotic expansion of (6) shows that as $\overline{\gamma} \to +\infty$, $\gamma_o \to 1$. Our numerical results show that γ_o increases as $\overline{\gamma}$ increases, which implies that γ_o always lies in the interval [0,1].

Substituting (2) in (3), and defining the integral $\mathcal{J}_n(\mu)$ as

$$\mathcal{J}_n(\mu) = \int_1^{+\infty} t^{n-1}\,\ln(t)\,e^{-\mu\,t}\,dt; \qquad \mu > 0, \tag{9}$$

we can rewrite the channel capacity $< C >_{\text{opra}}$ as

$$< C >_{\text{opra}} = \frac{W\,\log_2(e)}{\Gamma(m)}\left(\frac{m\,\gamma_o}{\overline{\gamma}}\right)^m \mathcal{J}_m\left(\frac{m\,\gamma_o}{\overline{\gamma}}\right). \tag{10}$$

The evaluation of $\mathcal{J}_n(\mu)$ for n a positive integer is derived in [14, Appendix A]. Using that result we obtain the NMF channel capacity per unit bandwidth $< C >_{\text{opra}} / W$ [bits/sec/Hz] under the optimal power and rate adaptation policy as

$$\frac{< C >_{\text{opra}}}{W} = \log_2(e) \sum_{k=0}^{m-1} \frac{\Gamma\left(k, m\,\frac{\gamma_o}{\overline{\gamma}}\right)}{k!}, \tag{11}$$

which can also be written as

$$\frac{< C >_{\text{opra}}}{W} = \log_2(e)\left(E_1(m\gamma_o/\overline{\gamma}) + \sum_{k=1}^{m-1} \frac{\mathcal{P}_k(m\gamma_o/\overline{\gamma})}{k}\right), \tag{12}$$

where $\mathcal{P}_k(.)$ denotes the Poisson distribution defined by,

$$\mathcal{P}_k(\mu) = e^{-\mu} \sum_{j=0}^{k-1} \frac{\mu^j}{j!}. \tag{13}$$

For the special case of the Rayleigh fading channel, using (7) in (12) for m=1, the optimal capacity per unit bandwidth reduces to the simple expression

$$\frac{< C >_{\text{opra}}}{W} = \log_2(e)\ \left(\frac{e^{-\gamma_o/\overline{\gamma}}}{\gamma_o/\overline{\gamma}} - \overline{\gamma}\right). \tag{14}$$

Using (2) in the probability of outage equation (5) yields

$$P_{\text{out}} = 1 - \frac{\Gamma(m, m\gamma_o/\overline{\gamma})}{\Gamma(m)} = 1 - \mathcal{P}_m(m\ \gamma_o/\overline{\gamma}). \tag{15}$$

3.2. Constant Transmit Power

With optimal rate adaptation to channel fading and with a constant transmit power, the channel capacity $< C >_{\text{ora}}$ [bits/sec] becomes [9]

$$< C >_{\text{ora}} = W \int_0^{+\infty} \log_2(1+\gamma)\ p_\gamma(\gamma)\, d\gamma. \tag{16}$$

$< C >_{\text{ora}}$ was previously introduced by Lee [15, 16] as the average channel capacity of a flat-fading channel, since it is obtained by averaging the capacity of an AWGN channel

$$C_{\text{awgn}} = W\ \log_2(1+\gamma) \tag{17}$$

over the distribution of the received CNR. In fact, (16) represents the capacity of the fading channel without transmitter feedback (i.e. with the channel fade level known at the receiver only) [17–19].

Substituting (2) into (16) and defining the integral $\mathcal{I}_n(\mu)$ as

$$\mathcal{I}_n(\mu) = \int_0^{+\infty} t^{n-1}\ \ln(1+t)\ e^{-\mu\ t}\ dt; \qquad \mu > 0, \tag{18}$$

the channel capacity $< C >_{\text{ora}}$ of a NMF channel can be written as

$$< C >_{\text{ora}} = \frac{W\ \log_2(e)}{\Gamma(m)}\ \left(\frac{m}{\overline{\gamma}}\right)^m\ \mathcal{I}_m\left(\frac{m}{\overline{\gamma}}\right). \tag{19}$$

The evaluation of $\mathcal{I}_n(\mu)$ for n a positive integer is derived in [14, Appendix B]. Using that result, we can rewrite $< C >_{\text{ora}} / W$ [bits/sec/Hz] as

$$\frac{< C >_{\text{ora}}}{W} = \log_2(e)\ e^{m/\overline{\gamma}} \sum_{k=0}^{m-1} \left(\frac{m}{\overline{\gamma}}\right)^k\ \Gamma\left(-k, \frac{m}{\overline{\gamma}}\right). \tag{20}$$

One may also express (18) in terms of the Poisson distribution as [16, Appendix] resulting in

$$\frac{< C >_{\text{ora}}}{W} = \log_2(e)\ \left(\mathcal{P}_m(-m/\overline{\gamma})\ E_1(m/\overline{\gamma}) + \sum_{k=1}^{m-1} \frac{\mathcal{P}_k(m/\overline{\gamma})\ \mathcal{P}_{m-k}(-m/\overline{\gamma})}{k}\right). \tag{21}$$

Note that Yao and Sheikh [20] as well as Buz [21] provided alternate closed-form expressions for the capacity of NMF channels. However their derivations are different than ours and their

resulting expressions [20, (7)] and [21, (1)] contain $m-1$ order derivatives. For the special case of the Rayleigh fading channel ($m=1$), (20) reduces to

$$\frac{<C>_{\text{ora}}}{W} = \log_2(e)\, e^{1/\overline{\gamma}}\, E_1(1/\overline{\gamma}). \tag{22}$$

3.3. Channel Inversion with Fixed Rate

The channel capacity when the transmitter adapts its power to maintain a constant CNR at the receiver (i.e., inverts the channel fading) was also investigated in [9]. This technique uses fixed-rate modulation and a fixed code design, since the channel after channel inversion appears as a time-invariant AWGN channel. As a result, channel inversion with fixed rate is the least complex technique to implement, assuming good channel estimates are available at the transmitter and receiver. The channel capacity with this technique ($<C>_{\text{cifr}}$ [bits/sec]) is derived from the capacity of an AWGN channel and is given in [9] as

$$<C>_{\text{cifr}} = W\, \log_2\left(1+\frac{1}{\int_0^{+\infty} p_\gamma(\gamma)/\gamma\, d\gamma}\right). \tag{23}$$

Channel inversion with fixed rate suffers a large capacity penalty relative to the other techniques, since a large amount of the transmitted power is required to compensate for the deep channel fades. Another approach is to use a modified inversion policy which inverts the channel fading only above a fixed cutoff fade depth γ_o. The capacity with this truncated channel inversion and fixed rate policy ($<C>_{\text{tifr}}$ [bits/sec]) was derived in [9] to be

$$<C>_{\text{tifr}} = W\, \log_2\left(1+\frac{1}{\int_{\gamma_o}^{+\infty} p_\gamma(\gamma)/\gamma\, d\gamma}\right)\, (1-P_{\text{out}}), \tag{24}$$

where P_{out} is given by (5). The cutoff level γ_o can be selected to achieve a specified outage probability or, alternatively (as shown in Figures 2, 3, and 4), to maximize (24).

By substituting the CNR distribution (2) in (23) we find that the capacity per unit bandwidth of an NMF channel with total channel inversion, $<C>_{\text{cifr}}/W$, is given for all $m \geq 1$ by

$$\frac{<C>_{\text{cifr}}}{W} = \log_2\left(1+\frac{m-1}{m}\,\overline{\gamma}\right). \tag{25}$$

Thus the capacity of a Rayleigh fading channel ($m=1$) is zero in this case. Note that the capacity of this policy for an NMF channel is the same as the capacity of an AWGN channels with equivalent CNR=$\frac{m-1}{m}\overline{\gamma}$.

With truncated channel inversion the capacity per unit bandwidth $<C>_{\text{tifr}}/W$ [bits/sec/Hz] can be expressed in terms of $\overline{\gamma}$ and γ_o by substituting (2) into (24), which yields

$$\frac{<C>_{\text{tifr}}}{W} = \log_2\left(1+\frac{\overline{\gamma}\,\Gamma(m)}{m\,\Gamma(m-1, m\gamma_o/\overline{\gamma})}\right)\frac{\Gamma(m, m\gamma_o/\overline{\gamma})}{\Gamma(m)}, \quad \forall m \geq 1. \tag{26}$$

For the special case of the Rayleigh fading channel ($m=1$), the capacity per unit bandwidth with truncated channel inversion reduces to

$$\frac{<C>_{\text{tifr}}}{W} = \log_2\left(1+\frac{\overline{\gamma}}{E_1(\gamma_o/\overline{\gamma})}\right)\, e^{-\gamma_o/\overline{\gamma}}. \tag{27}$$

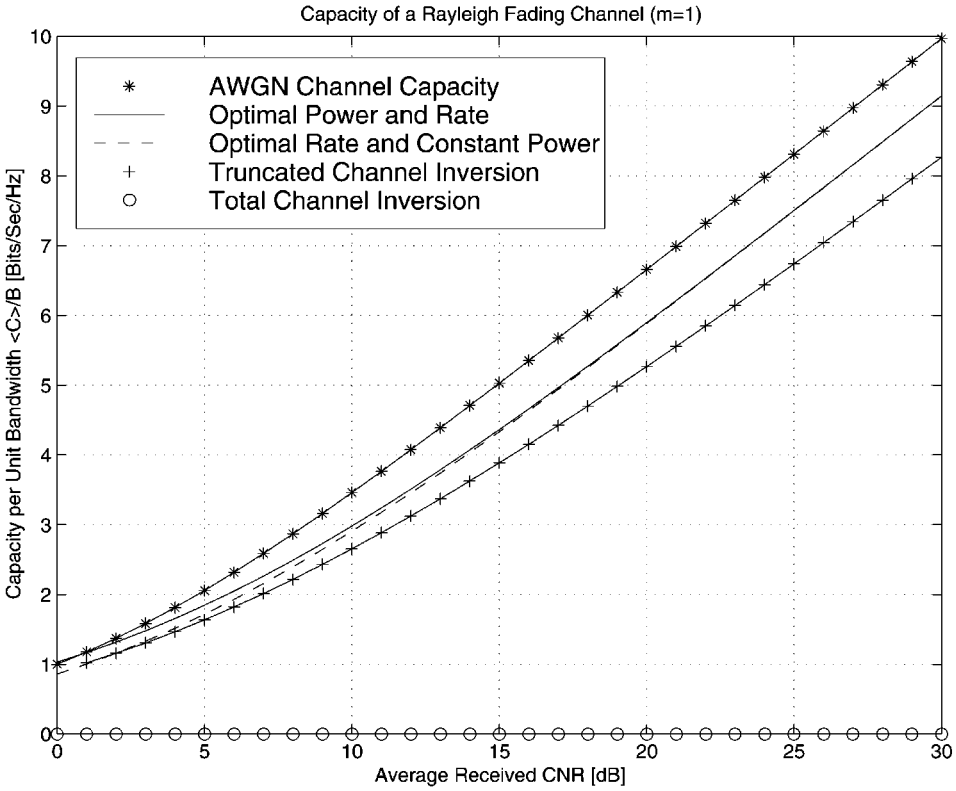

Figure 2. Capacity per unit bandwidth for a Rayleigh fading channel ($m = 1$) under different adaption policies.

3.4. NUMERICAL RESULTS

Figures 2, 3, and 4 show the capacity per unit bandwidth as a function of $\overline{\gamma}$ for a NMF channel under the three different adaptive policies for $m = 1$ (Rayleigh channel), $m = 2$, and $m = 4$, respectively. We see from these figures that the capacity of NMF channels is always smaller than the capacity of an AWGN channel for $\overline{\gamma} \geq 0$ dB but converges to it as the m parameter increases or, equivalently, as the amount of fading decreases. We also see that optimal power and rate adaptation yields a small increase in capacity over just optimal rate adaptation, and this small increase in capacity diminishes as the average received CNR and/or fading parameter m increases. Recall that the capacity with just rate adaptation is the same as the capacity of a non-adaptive system with only receiver information. Hence these numerical results also show that transmitter adaptation with respect to channel variations provides very little capacity gain over non-adaptive systems. Note finally that fixed rate transmission with channel inversion suffers the largest capacity penalty. However, this penalty diminishes as the amount of fading decreases.

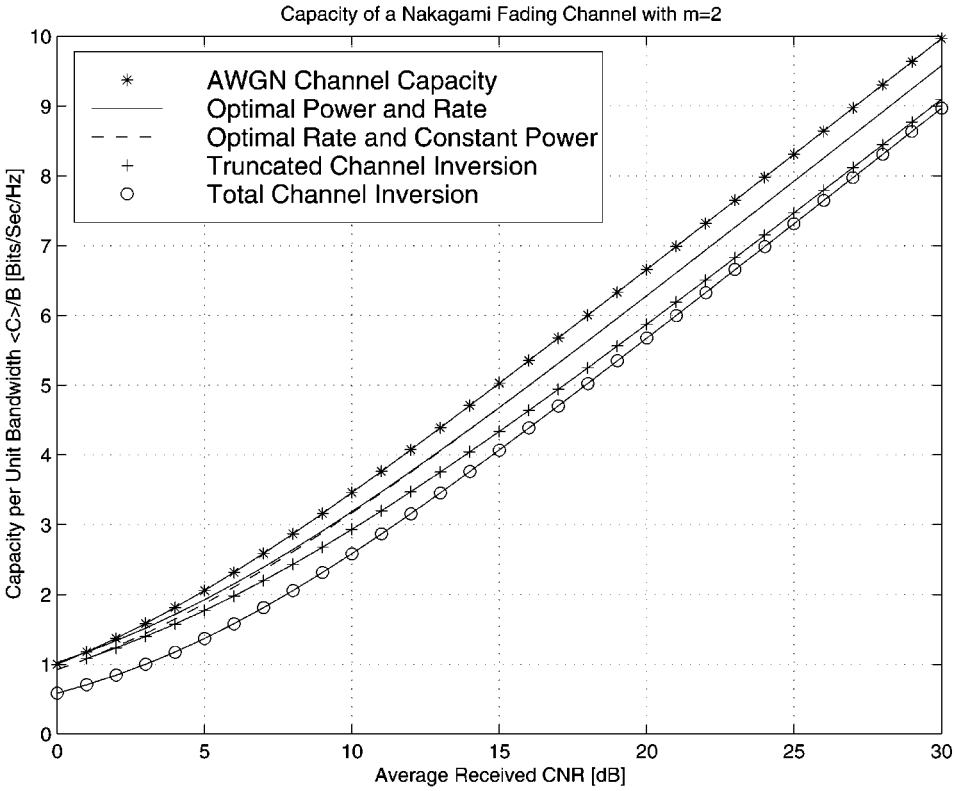

Figure 3. Capacity per unit bandwidth for a Nakagami fading channel with $m = 2$, and for different adaption policies.

4. Adaptive M-QAM Modulation

4.1. Proposed Adaptive Schemes

The BER of coherent M-QAM with two-dimensional Gray coding over an additive white Gaussian noise (AWGN) channel assuming perfect clock and carrier recovery can be well approximated by [6]

$$\mathrm{BER}(M, \gamma) \simeq 0.2 \ \exp\left(-\frac{3\,\gamma}{2\,(M-1)}\right). \tag{28}$$

Exact expressions for the BER of "square" M-QAM (when the number of bits per symbol n is even) are known [22, Chapter 5], and are plotted by the solid lines in Figure 5. On the other hand, tight upper-bounds on the BER of "non-square" M-QAM (when the number of bits per symbol n is odd) are also available [23, p. 283], and are plotted by the cross/solid lines in Figure 5. For comparison, the dashed lines in this figure show the BER approximation (28) for different values of M. Note that the approximate BER expression upper bounds the exact BER for $M \geq 4$ and for BER $\leq 10^{-2}$, which is the BER range of interest. We will use this approximation when needed in our analysis since it is "invertible" in the sense that it provides a simple closed-form expression for the link spectral efficiency of M-QAM as a function of the CNR and the BER. In addition, (28) and its inverse are very simple functions which lead,

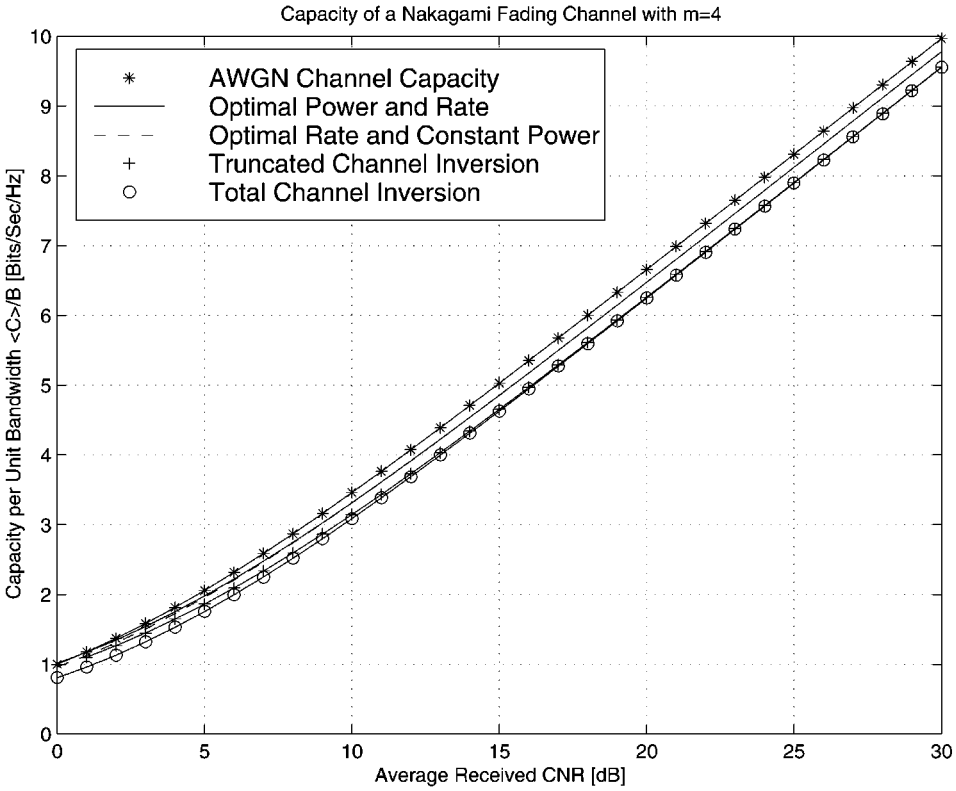

Figure 4. Capacity per unit bandwidth for a Nakagami fading channel with $m = 4$, and for different adaption policies.

as shown below, to closed-form analytical expressions and insights that are unattainable with more complicated BER expressions.

Assuming ideal Nyquist pulses and given a fixed CNR (γ) and BER (BER_0), the spectral efficiency of continuous-rate M-QAM can be approximated by inverting (28), giving

$$\frac{R}{W} = \log_2(M) = \log_2\left(1 + \frac{3\,\gamma}{2\,K_0}\right), \tag{29}$$

where $K_0 = -\ln(5\ \text{BER}_0)$. The adaptive continuous rate (ACR) M-QAM scheme responds to the instantaneous channel CNR fluctuation by varying the number of bits per symbol according to (29). In the context of this paper, continuous-rate means that the number of bits per symbol is not restricted to integer values. While continuous-rate M-QAM is possible [24], it is more practical to study the performance of adaptive discrete rate (ADR) M-QAM, where the constellation size M_n is restricted to 2^n for n a positive integer. In this case the scheme responds to the instantaneous channel CNR fluctuation by varying its constellation size as follows. The CNR range is divided into $N + 1$ *fading regions*, and the constellation size M_n is assigned to the nth region ($n = 0, 1, \cdots, N$). When the received CNR is estimated to be in the nth region, the constellation size M_n is transmitted.

Suppose we set a target BER equal to BER_0. The region boundaries (or switching thresholds) $\{\gamma_n\}$ are then set to the CNR required to achieve the target BER_0 using M_n-QAM

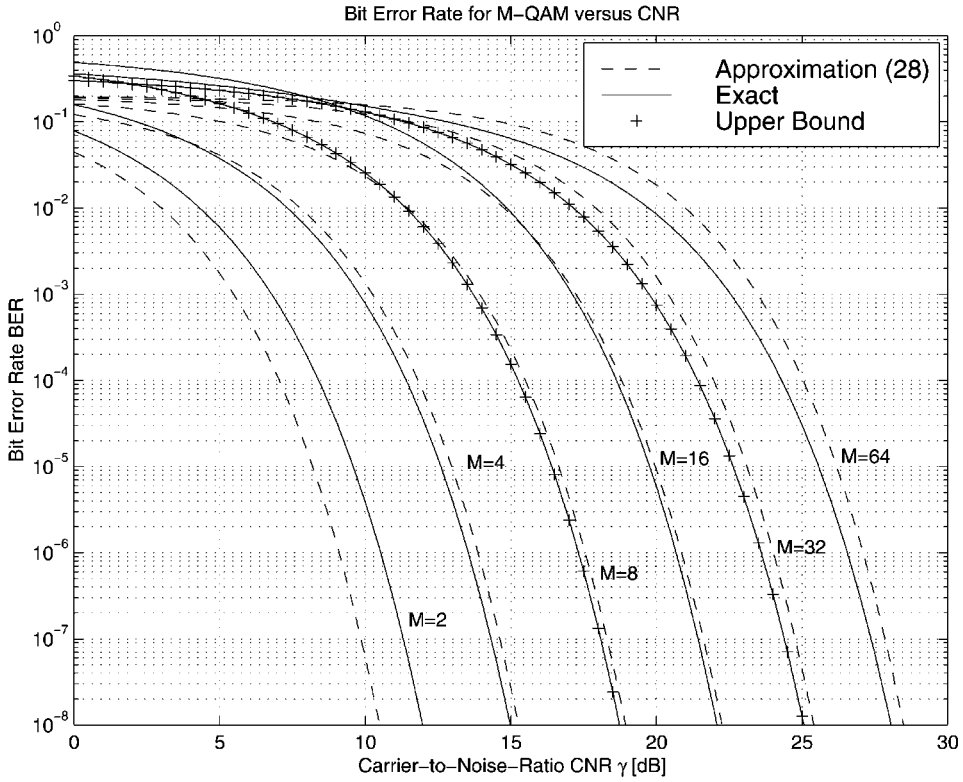

Figure 5. BER for M-QAM versus CNR.

over an AWGN channel. Specifically

$$\begin{aligned} \gamma_1 &= [\text{erfc}^{-1}(2\,\text{BER}_0)]^2, \\ \gamma_n &= \frac{2}{3}\,K_0\,(2^n - 1); \qquad n = 0, 2, 3, \cdots, N, \\ \gamma_{N+1} &= +\infty, \end{aligned} \tag{30}$$

where $\text{erfc}^{-1}(.)$ denotes the inverse complementary error function. When the switching thresholds are chosen according to (30), the system will operate with a BER below the target BER, as will be confirmed in Section 4.4. Note in particular that all the γ_ns (except γ_1) are chosen according to (28). Since (28) is an upper-bound of the BER only for $M \geq 4$, γ_1 is chosen according to the exact BER performance of 2-QAM (BPSK). The thick line in Figure 6 shows the number of bits per symbol as a function of the received CNR for ADR M-QAM with 8-regions, along with the corresponding switching thresholds. For comparison the thin line in this figure shows the bits per symbol of ACR M-QAM.

4.2. Outage Probability

Since no data is sent when the received CNR falls below γ_1, the ADR M-QAM scheme suffers an outage probability, P_{out}, of

$$P_{\text{out}} = \int_0^{\gamma_1} p_\gamma(\gamma)\,d\gamma = 1 - \frac{\Gamma\left(m, \frac{m\gamma_1}{\bar{\gamma}}\right)}{\Gamma(m)}. \tag{31}$$

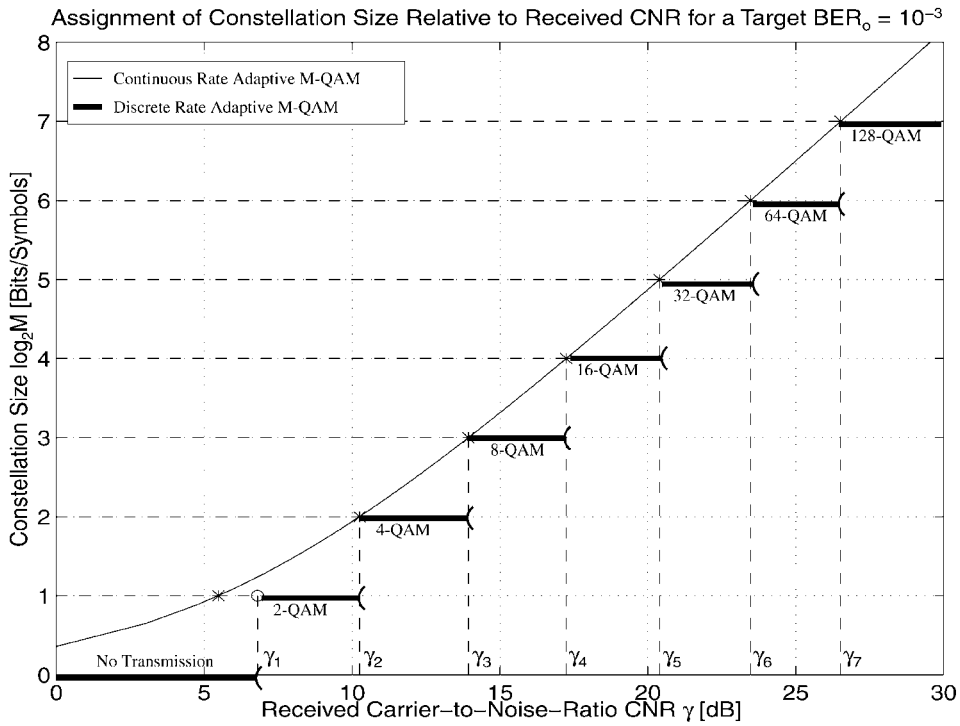

Figure 6. Number of bits per symbol versus CNR.

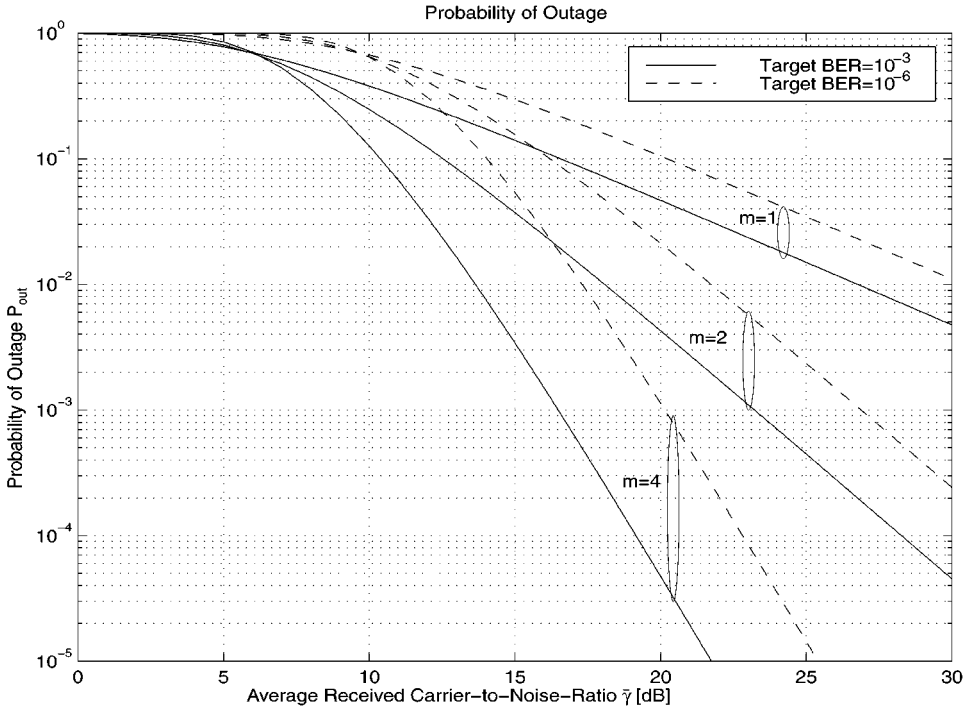

Figure 7. Outage probability in Nakagami fading.

Figure 7 shows the outage probability for various values of the Nakagami fading parameter and for target BERs of 10^{-3} and 10^{-6}, respectively.

4.3. Achievable Spectral Efficiency

Integrating (29) over (2) and following the same steps of Section 3.2 which obtained (20), we find the average link spectral efficiency, $< R >_{\text{acr}} / W$, of the ACR M-QAM over NMF channels as

$$\frac{< R >_{\text{acr}}}{W} = \frac{e^{\frac{2mK_0}{3\overline{\gamma}}}}{\ln(2)} \sum_{k=0}^{m-1} \left(\frac{2mK_0}{3\overline{\gamma}}\right)^k \Gamma\left(-k, \frac{2mK_0}{3\overline{\gamma}}\right). \tag{32}$$

The average link spectral efficiency, $< R >_{\text{adr}} / W$, of the ADR M-QAM over NMF channels is just the sum of the data rates ($\log_2[M_n] = n$) associated with the individual $N+1$ regions, weighted by the probability $a_n = \int_{\gamma_n}^{\gamma_{n+1}} p_\gamma(\gamma)\, d\gamma$ that the CNR γ falls in the nth region:

$$\frac{< R >_{\text{adr}}}{W} = \sum_{n=1}^{N} n\, a_n, \tag{33}$$

where the a_ns can be expressed as

$$a_n = \frac{\Gamma\left(m, \frac{m\,\gamma_n}{\overline{\gamma}}\right) - \Gamma\left(m, \frac{m\,\gamma_{n+1}}{\overline{\gamma}}\right)}{\Gamma(m)}. \tag{34}$$

Figures 8, 9, and 10 show the average link spectral efficiency of ACR M-QAM (32) and ADR M-QAM (33) for a target $\text{BER}_0 = 10^{-3}$ and for m=1, $m = 2$, and $m = 4$, respectively. The Shannon capacity using constant-power and variable-rate (20) is also shown for comparison, along with the spectral efficiency of nonadaptive 2-QAM (BPSK). This latter efficiency is found by determining the value of the average received CNR for which the average BER of nonadaptive BPSK over Nakagami fading channel, as given by (38), equals the target BER. Note that for a target BER of 10^{-3} the achievable spectral efficiency of ACR M-QAM comes within 5 dB of the Shannon capacity limit. ADR M-QAM suffers a minimum additional 1.2 dB penalty, whereas nonadaptive uncoded BPSK suffers a large spectral efficiency penalty. Hence contrary to the capacity results (which do not have any complexity constraints), adaptive systems perform much better than non-adaptive ones in uncoded situations. This implies that the gain of adaptive systems over non-adaptive ones vary inversely with the system coding complexity.

4.4. Average Bit Error Rate

ACR M-QAM always operates at the target BER. However, since the choice of M_n in ADR M-QAM is done in a conservative fashion, this discrete technique operates at an average BER, $< \text{BER} >_{\text{adr}}$, smaller than the target BER. This BER can be computed exactly as the ratio of the average number of bits in error over the total average number of transmitted bits:

$$< \text{BER} >_{\text{adr}} = \frac{\sum_{n=1}^{N} n\, \overline{\text{BER}}_n}{\sum_{n=1}^{N} n\, a_n}, \tag{35}$$

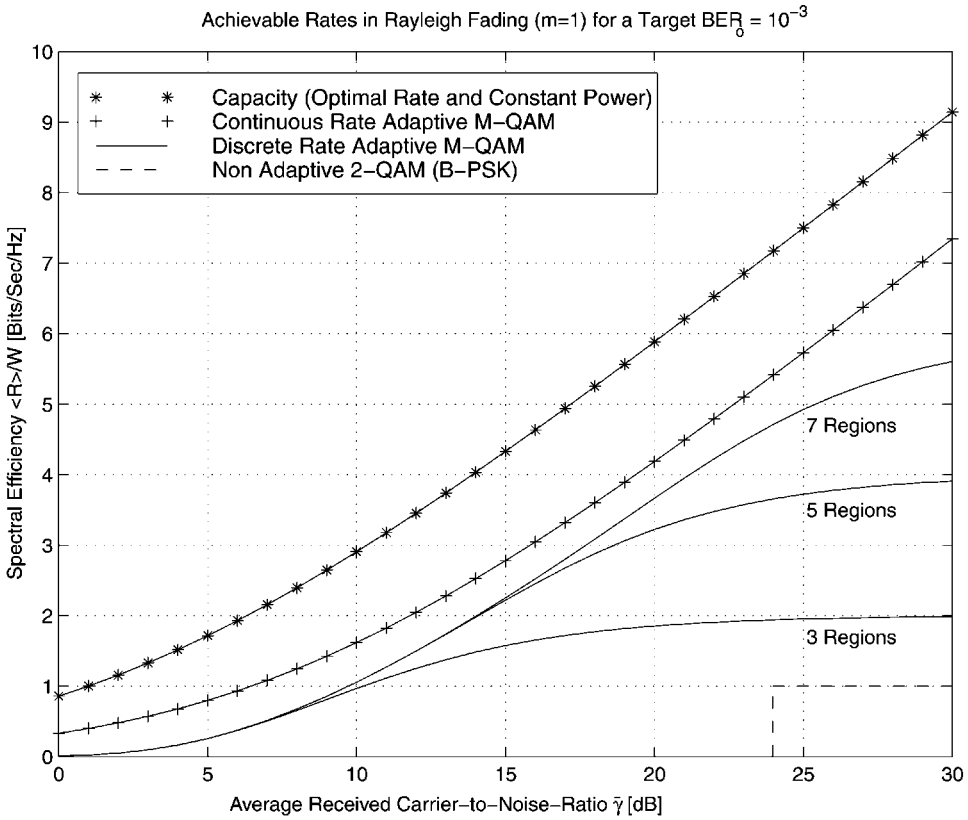

Figure 8. Achievable spectral efficiency for a target BER of 10^{-3} and $m = 1$ (Rayleigh fading).

where

$$\overline{\text{BER}}_n = \int_{\gamma_n}^{\gamma_{n+1}} \text{BER}(M_n, \gamma)\ p_\gamma(\gamma)\ d\gamma. \tag{36}$$

Using (2) and the approximation (28) in (36) $\overline{\text{BER}}_n$ can be expressed in closed-form as

$$\overline{\text{BER}}_n = \frac{0.2}{\Gamma(m)} \left(\frac{m}{\overline{\gamma}}\right)^m \frac{\Gamma(m, b_n\gamma_n) - \Gamma(m, b_n\gamma_{n+1})}{(b_n)^m}, \tag{37}$$

where

$$b_n = \frac{m}{\overline{\gamma}} + \frac{3}{2\ (2^n - 1)}; \qquad n = 1, 2, \cdots, N.$$

$\overline{\text{BER}}_n$ can also be computed exactly by using the exact expressions for the $\text{BER}(M_n, \gamma)$ as given in [22, Chapter 5] and [10].

Figures 11, 12, and 13 show the average BER for ADR M-QAM for a target BER of 10^{-3} and for $m = 1$, $m = 2$, and $m = 4$, respectively. The BER calculations based on the approximation (37) are plotted as solid lines whereas the exact average BERs are plotted as star/solid lines. The average BER of nonadaptive uncoded BPSK over Nakagami fading channel is given by [25, Appendix A]

$$<\text{BER}>_{\text{bpsk}} = \frac{1}{2}\sqrt{\frac{\overline{\gamma}}{\pi}}\ \frac{m^m}{(m+\overline{\gamma})^{m+1/2}} \frac{\Gamma(m+1/2)}{\Gamma(m+1)}\ {}_2F_1\left(1, m+1/2; m+1; \frac{m}{m+\overline{\gamma}}\right), \tag{38}$$

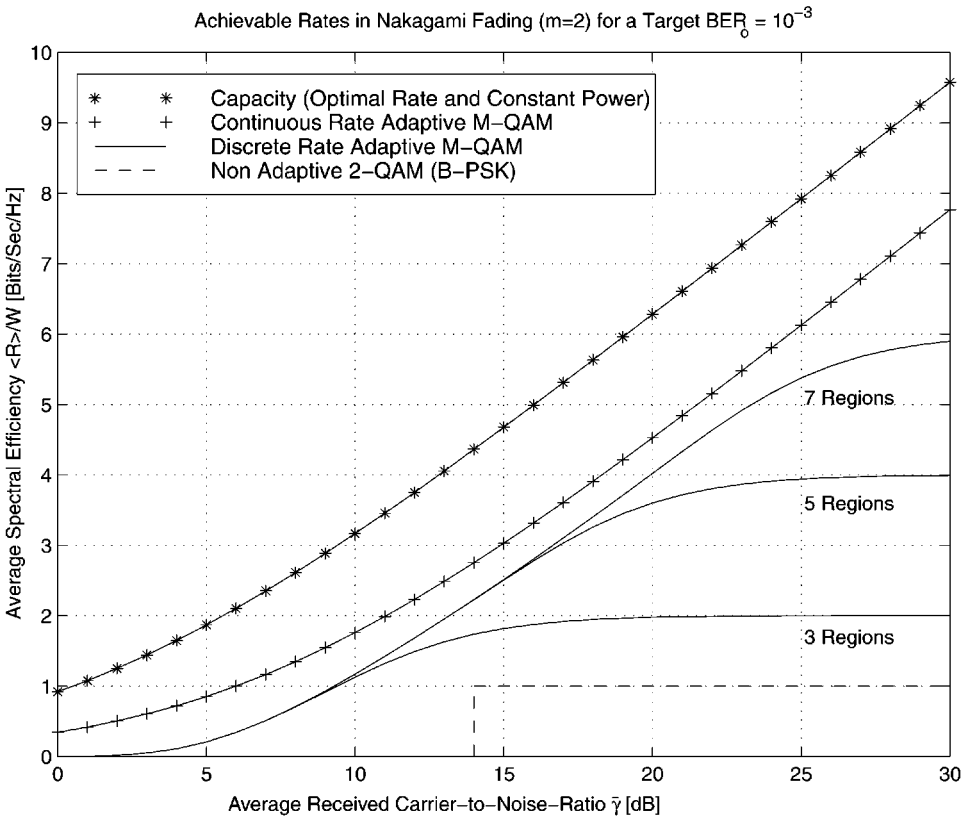

Figure 9. Achievable spectral efficiency for a target BER of 10^{-3} and $m = 2$.

where ${}_2F_1(.,.;.;.)$ denotes the Gauss' hypergeometric function [11]. We plot (38) in Figures 11, 12, and 13 in dashed lines for comparison with (35).

In these figures we observe similar trends in the average BER for various values of the m parameter. For instance, we see that the average BER of ADR M-QAM is well beneath the 10^{-3} target BER. This is due to the fact that the thresholds $\gamma_1, \gamma_2, \cdots, \gamma_N$ are chosen so that the instantaneous BER is guaranteed to be always lower then the target BER. Clearly this conservative design choice can be relaxed and the predetermined thresholds can be optimized so that only the average BER is lower than the target BER [26]. In that case higher spectral efficiency can be achieved. Recall that the approximation (28) lower bounds the exact BER for M=2 and that ADR M-QAM often uses the 2-QAM constellation (B-PSK) at low average CNRs. This explains why the average BER based on the approximation (37) lower bounds the exact average BER for $\overline{\gamma} \leq 10$ dB. Conversely, because of the fact that the approximation (28) upper bounds the exact BER for $M > 2$ and because ADR M-QAM often uses the high constellation sizes at high average CNRs, the closed-form approximate average BER for ADR M-QAM tightly upper-bounds the exact average BER for $\overline{\gamma} \geq 10$ dB. Since ADR M-QAM uses the largest available constellation often when the average CNR is large, the average BER prediction as $\overline{\gamma}$ increases becomes dominated by the BER performance of that constellation.

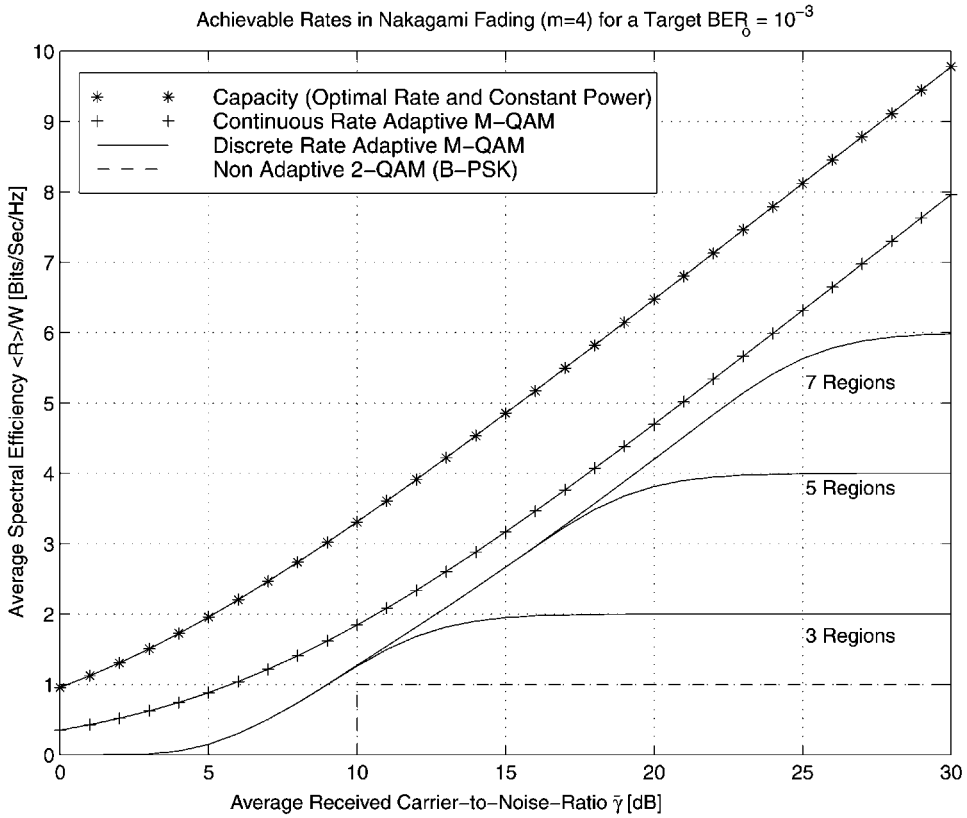

Figure 10. Achievable spectral efficiency for a target BER of 10^{-3} and $m = 4$.

5. Impact of Time Delay

Recall from Section 2.1 that the choice of the constellation size is based on a channel estimate at time t, whereas the data are sent over the channel at time $t + \tau$ such that $\tau_{fb} \leq \tau \leq \tau_t$. If a delay of τ_{fb} degrades BER significantly, then this adaptive technique will not work, since τ_{fb} is an inherent and unavoidable parameter of the system. However, if a delay of $\tau \geq \tau_{fb}$ has a small impact on the BER then we should choose τ_t as large as possible so that we meet the BER requirement while minimizing the rate of system reconfiguration. In this section we analyze the impact of time delay on the performance of adaptive M-QAM over NMF channels, assuming perfect channel estimates. Note that this issue has also been addressed in a recent paper [27] by Goeckel who considered the impact of channel variations on adaptive coded modulations over Rayleigh fading channels.

5.1. Fading Correlation

Investigating the impact of time delay requires the second-order statistics for the channel variation, which are known for Nakagami fading. Let α and α_τ denote the channel gains at a time t and $t + \tau$, respectively. For a slowly-varying channel we can assume that the *average* received power remains constant over the time delay τ (i.e., $\Omega = E(\alpha^2) = E(\alpha_\tau^2)$). Under

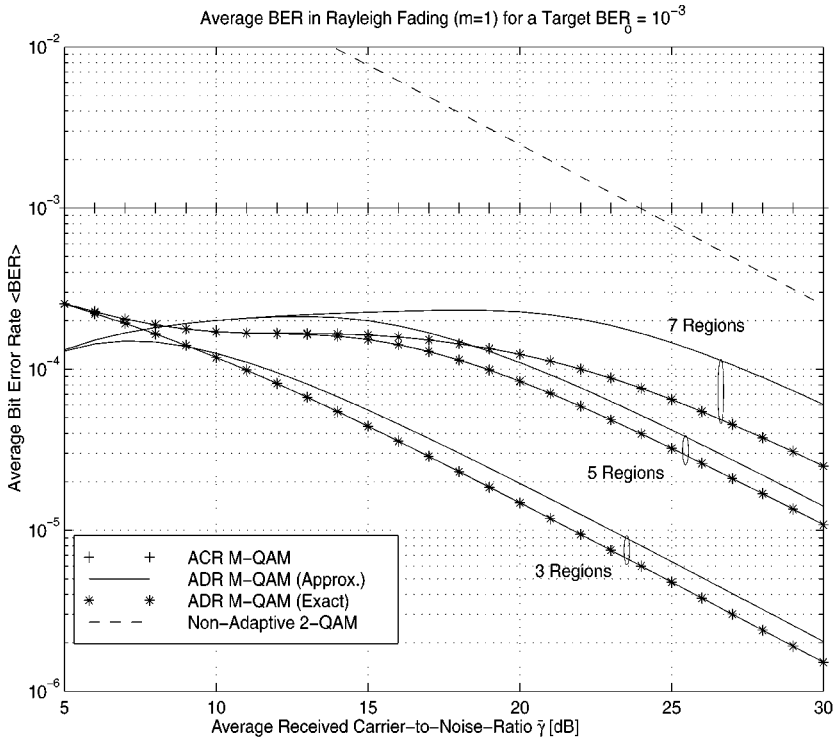

Figure 11. Average BER for a target BER of 10^{-3} and $m = 1$ (Rayleigh).

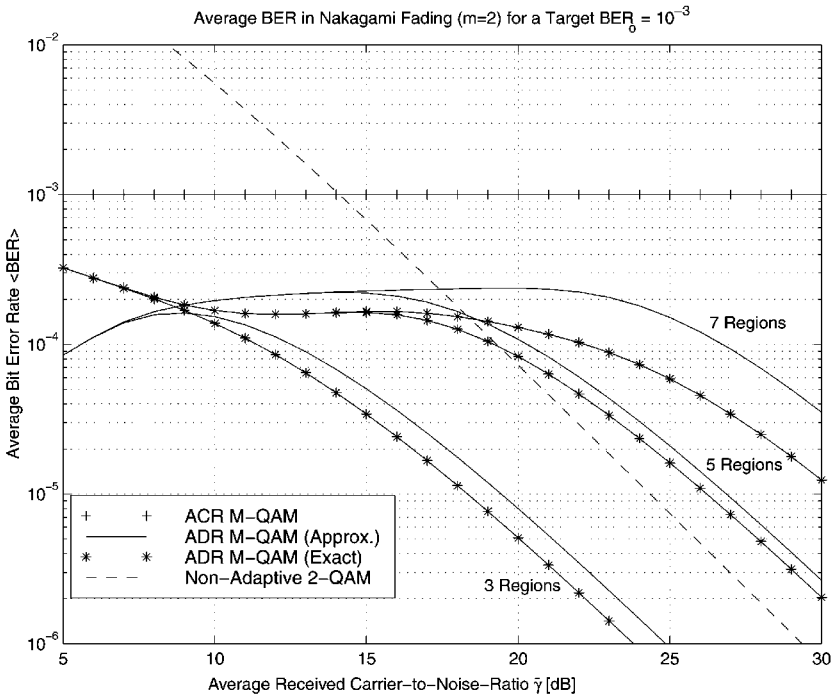

Figure 12. Average BER for a target BEr of 10^{-3} and $m = 2$.

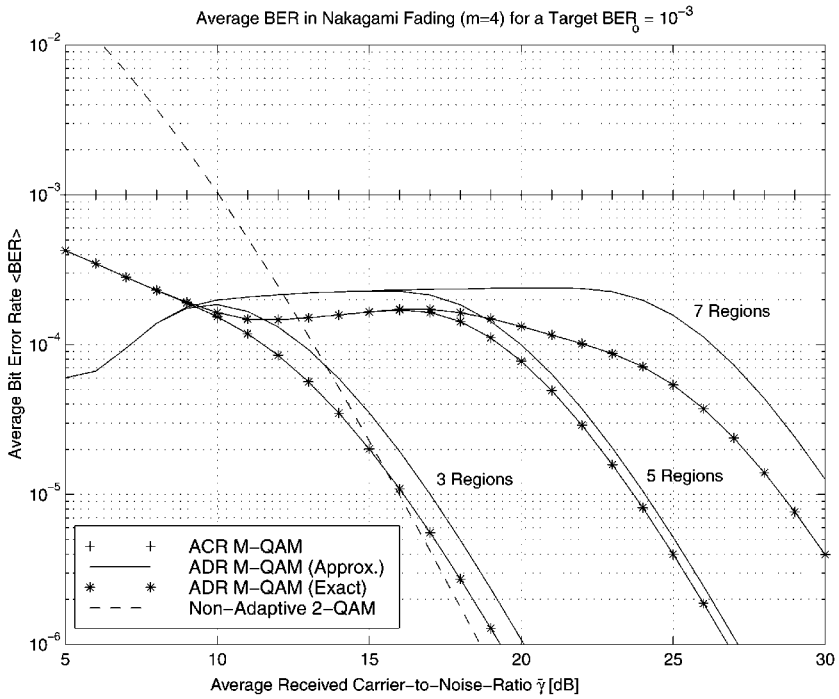

Figure 13. Average BER for a target BER of 10^{-3} and $m = 4$.

these conditions the joint PDF $p_{\alpha,\alpha_\tau}(\alpha, \alpha_\tau)$ of these two correlated Nakagami-m distributed channel gains is given by [2, (126)]

$$p_{\alpha,\alpha_\tau}(\alpha, \alpha_\tau) = \frac{4\ (\alpha\ \alpha_\tau)^m}{(1-\rho)\ \Gamma(m)\ \rho^{(m-1)/2}} \left(\frac{m}{\Omega}\right)^{m+1}\ I_{m-1}\left(\frac{2m\sqrt{\rho}\ \alpha\alpha_\tau}{(1-\rho)\Omega}\right) \exp\left(-\frac{m\ (\alpha^2+\alpha_\tau^2)}{(1-\rho)\ \Omega}\right), \quad (39)$$

where $I_{m-1}(.)$ is the $(m-1)th$-order modified Bessel function of the first kind [11], and ρ is the correlation factor between α and α_τ. Since Nakagami fading assumes isotropic scattering of the multipath components, ρ can be expressed in terms of the time delay τ, the mobile speed, v [m/s], and the wavelength of the carrier frequency λ_c [m] as $\rho = J_0^2(2\pi f_D \tau)$, where $J_0(.)$ is the zero-order Bessel function of the first kind [11], and $f_D = v/\lambda_c$ [Hz] is the maximum Doppler frequency shift [28, p. 31].

The PDF of α_τ conditioned on α, $p_{\alpha_\tau/\alpha}(\alpha_\tau/\alpha)$, is given by

$$p_{\alpha_\tau/\alpha}(\alpha_\tau/\alpha) = \frac{p_{\alpha_\tau,\alpha}(\alpha_\tau, \alpha)}{p_\alpha(\alpha)}. \quad (40)$$

Inserting (1) and (39) in (40) and expressing the result in terms of the CNRs γ and γ_τ yields

$$p_{\gamma_\tau/\gamma}(\gamma_\tau/\gamma) = \frac{m}{(1-\rho)\overline{\gamma}} \left(\frac{\gamma_\tau}{\rho\ \gamma}\right)^{(m-1)/2}\ I_{m-1}\left(\frac{2m\sqrt{\rho\gamma\gamma_\tau}}{(1-\rho)\ \overline{\gamma}}\right)\ \exp\left(-\frac{m(\rho\gamma+\gamma_\tau)}{(1-\rho)\ \overline{\gamma}}\right). \quad (41)$$

5.2. ANALYSIS

5.2.1. *Adaptive Continuous Rate M-QAM*

For all delays τ let the communication system be configured according to γ (CNR at $\tau = 0$) such that $M(\gamma)$ is given by

$$M(\gamma) = 1 + \frac{3\,\gamma}{2\,K_0}. \tag{42}$$

The constellation size $M(\gamma)$ is based on the value γ at time t, but that constellation is transmitted over the channel at time $t + \tau$, when γ has changed to γ_τ. Since M does not depend on γ_τ (CNR at time τ), time delay does not affect the link spectral efficiency $< \log_2 M >$, as calculated in Section IV-C. However, delay affects the instantaneous BER, which becomes a function of the "mismatch" between γ_τ and γ:

$$\mathrm{BER}(\gamma_\tau/\gamma) = \mathrm{BER}(M(\gamma), \gamma_\tau) = 0.2\,(5\,\mathrm{BER_o})^{\gamma_\tau/\gamma}. \tag{43}$$

Integrating (43) over the conditional PDF (41) yields the average BER conditioned on γ, $\mathrm{BER}(\gamma)$, as

$$\mathrm{BER}(\gamma) = \int_0^{+\infty} \mathrm{BER}(\gamma_\tau/\gamma)\; p_{\gamma_\tau/\gamma}(\gamma_\tau/\gamma)\; d\gamma_\tau. \tag{44}$$

Inserting (41) and (43) in (44), and using the change of variable $z = \left(\frac{K_0}{\gamma} + \frac{m}{\overline{\gamma}(1-\rho)}\right)\gamma_\tau$, $\mathrm{BER}(\gamma)$ can be written in closed-form with the help of the generalized Marcum Q-function of order m, $Q_m(.,.)$ defined by [29, p. 299, (11.63)]

$$Q_m(\alpha, \beta) = \frac{1}{\alpha^{m-1}} \int_\beta^\infty z^m \exp\left[-\left(\frac{z^2+\alpha^2}{2}\right)\right]\; I_{m-1}(\alpha z)\; dz$$

as

$$\begin{aligned}\mathrm{BER}(\gamma) = {} & 0.2\left(\frac{m\,\gamma}{m\,\gamma + \overline{\gamma}\,(1-\rho)\,K_0}\right)^m \exp\left(-\frac{\rho\,K_0\,m\,\gamma}{m\,\gamma + \overline{\gamma}\,(1-\rho)\,K_0}\right) \times \\ & \times Q_m\left(\frac{\rho\,m^2\,\gamma^2}{\overline{\gamma}(1-\rho)(m\gamma + \overline{\gamma}(1-\rho)K_0)}, 0\right).\end{aligned} \tag{45}$$

Using the recurrence relation [29, p. 299, (11.64)]

$$Q_{m+1}(x, y) = Q_m(x, y) + \left(\frac{y}{x}\right)^{m/2}\; I_m(2\sqrt{xy})\; e^{-x}, \tag{46}$$

we get that for all x, $Q_m(x, 0) = Q_1(x, 0)$, which can be shown to equal 1. Therefore, $\mathrm{BER}(\gamma)$ reduces to:

$$\mathrm{BER}(\gamma) = 0.2\,\left(\frac{m\,\gamma}{m\,\gamma + \overline{\gamma}\,(1-\rho)\,K_0}\right)^m\; \exp\left(-\frac{\rho\,K_0\,m\,\gamma}{m\,\gamma + \overline{\gamma}\,(1-\rho)\,K_0}\right). \tag{47}$$

Although this formula was derived for integer m it is also valid for all non-integer values of $m \geq 1/2$. Averaging (47) over the PDF of γ (2) yields the average BER of ACR M-QAM, $< \mathrm{BER} >_{\mathrm{acr}}$, as

$$< \mathrm{BER} >_{\mathrm{acr}} = \int_{\gamma_1}^{+\infty} \mathrm{BER}(\gamma)\; p_\gamma(\gamma)\; d\gamma. \tag{48}$$

Finally, using (47) in (48) and making the substitution $u = \frac{m\ \gamma}{m\ \gamma+(1-\rho)K_0\overline{\gamma}}$ yields

$$< \text{BER} >_{\text{acr}} = \frac{0.2\ (1-\rho)^m\ K_0^m}{\Gamma(m)} \int_{u_1}^{1} \frac{u^{2m-1}}{(1-u)^{m+1}} \exp\left(-\frac{K_0 u(1-\rho u)}{1-u}\right) du, \tag{49}$$

where

$$u_1 = \frac{m\ \gamma_1}{m\ \gamma_1 + (1-\rho)K_0\overline{\gamma}}.$$

Since this analysis assumes continuous rate adaptation and since $M_n(\gamma) \leq M(\gamma)$ for all γ, (49) represents an upper-bound on the average BER degradation for ADR M-QAM, as will be confirmed in the following sections.

5.2.2. *Adaptive Discrete Rate M-QAM*

Suppose now that the constellation size M_n is chosen based on the value of γ according to the ADR M-QAM scheme described in Section 4.1. However the constellation is transmitted over the channel when γ has changed to γ_τ. As in Section 5.2.1, we can easily see that the link spectral efficiency of ADR M-QAM is unaffected by time delay. However, delay affects $< \text{BER} >_{\text{adr}}$, which is computed from (35) with $\overline{\text{BER}}_n$ replaced by $\overline{\text{BER}}_n^{'}$, where

$$\overline{\text{BER}}_n^{'} = \int_{\gamma_n}^{\gamma_{n+1}} \int_0^{\infty} \text{BER}(M_n, \gamma_\tau)\ p_{\gamma_\tau/\gamma}(\gamma_\tau/\gamma)\ d\gamma_\tau\ p_\gamma(\gamma)\ d\gamma.$$

Using again the generalized Marcum Q-functions, it can be shown that

$$\overline{\text{BER}}_n^{'} = \frac{0.2}{\Gamma(m)} \left(\frac{m}{\overline{\gamma}}\right)^m \frac{\Gamma(m, b_n'\gamma_n) - \Gamma(m, b_n'\gamma_{n+1})}{(b_n)^m}, \tag{50}$$

where

$$b_n' = \frac{m}{\overline{\gamma}} + \frac{3\ \rho\ m}{3(1-\rho)\overline{\gamma} + 2m(2^n - 1)}; \qquad n = 1, 2, \cdots, N.$$

Note that as $\rho \to 1$ (i.e., $\tau \to 0$), $b_n' \to b_n$, and $\overline{\text{BER}}_n^{'}$ (50) reduces to $\overline{\text{BER}}_n$ (37), as expected.

5.3. Numerical Results

Figures 14 and 15 show $< \text{BER} >_{\text{acr}}$ and $< \text{BER} >_{\text{adr}}$ as a function of the normalized time delay $f_D\tau$ for different values of the Nakagami m parameter, for a target BER of 10^{-3} and 10^{-6}, respectively. It can be seen from Figures 14 and 15 that a normalized time delay up to about 10^{-2} can be tolerated without a noticeable degradation in the average BER. For example, for a 900 MHz carrier frequency and a target BER of 10^{-3}, a time delay up to 3.33 ms can be tolerated for pedestrians with a speed of 1 m/s (3.6 km/hr), and a time delay up to 0.133 ms can be tolerated for mobile vehicles with a speed of 25 m/s (90 km/hr). Comparing Figures 14 and 15, we see that systems with the lower BER requirements of 10^{-6} are more sensitive to time delay, as they will suffer a higher "rate of increase" in BER. For example, in Rayleigh fading, systems with a 10^{-3} BER requirement suffer about one order of magnitude degradation for $f_D\tau$ between 10^{-2} and 10^{-1}, whereas systems with a 10^{-6} BER requirement suffer about four orders of magnitude degradation for the same range of $f_D\tau$. However, in

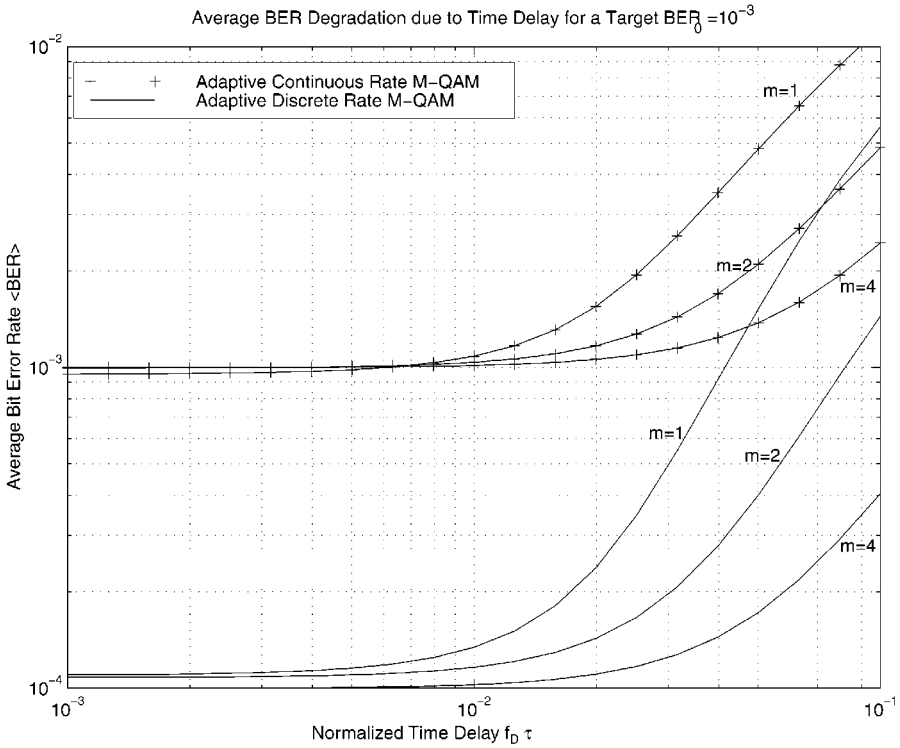

Figure 14. Average BER vs. normalized time delay for a BER_0 of 10^{-3}, $\bar{\gamma} = 20$ dB, and 5 fading regions.

both cases these systems will be able to operate satisfactorily if the normalized delay is below the critical value of 10^{-2}.

6. Conclusion

We have studied the capacity of NMF channels with an average power constraint for three power and rate adaptation policies. We obtain closed-form solutions for NMF channel capacity for each power and rate adaptation strategy. Our results show that optimal power and rate adaptation yields a small increase in capacity over just optimal rate adaptation with constant power or equivalently the capacity of non-adaptive systems, and this small increase in capacity diminishes as the average received carrier-to-noise ratio, and/or the m parameter increases. Fixed rate transmission with channel inversion suffers the largest capacity penalty. However, this penalty diminishes as the amount of fading decreases. We then proposed and studied the performance of practical constant-power variable-rate M-QAM schemes over NMF channels assuming perfect channel estimation and negligible time delay. We determined their spectral efficiency and compared this to the theoretical maximum. Our results show that for a target BER of 10^{-3}, the spectral efficiency of adaptive continuous rate M-QAM comes within 5 dB of the Shannon capacity limit and adaptive discrete rate M-QAM comes within 6.2 dB of this limit, whereas nonadaptive uncoded BPSK suffers a large spectral efficiency penalty. In view of the capacity results we can thus conclude that the gain of adaptive systems over non-adaptive ones vary inversely with the system coding complexity. We also analyzed the impact of time delay on the BER of adaptive M-QAM. Results show that systems with low BER

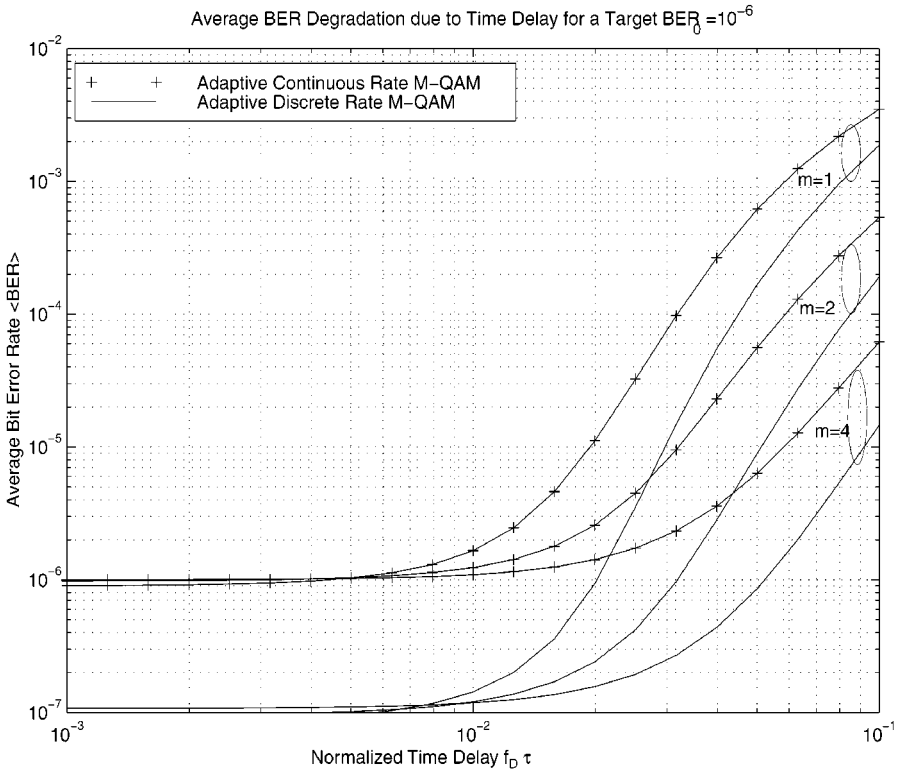

Figure 15. Average BER vs. normalized time delay for a BER_0 of 10^{-6}, $\bar{\gamma} = 20$ dB, and 5 fading regions.

requirements will be more sensitive to time delay but will still be able to operate satisfactorily if the normalized time delay is below the critical value of 10^{-2}.

Acknowledgements

The authors would like to thank the anonymous reviewers for their valuable comments and suggestions which enhanced the quality of the paper.

References

1. K. Pahlavan and A.H. Levesque, "Wireless Data Communications", *Proc. IEEE*, Vol. 82, pp. 1398–1430, 1994.
2. M. Nakagami, "The *m*-Distribution – A General Formula of Intensity Distribution of Rapid Fading", in *Statistical Methods in Radio Wave Propagation*, pp. 3–36, Pergamon Press: Oxford, U.K., 1960.
3. J.K. Cavers, "Variable-Rate Transmission for Rayleigh Fading Channels", *IEEE Trans. Commun.*, Vol. COM-20, pp. 15–22, 1972.
4. T. Ue, S. Sampei and N. Morinaga, "Symbol Rate and Modulation Level Controlled Adaptive Modulation/TDMA/TDD for Personal Communication Systems", in *Proc. IEEE Veh. Technol. Conf. VTC '95*, Chicago, IL, July 1995, pp. 306–310. Full paper published in the *IEICE Trans. Commun.*, Vol. E78-B, pp. 1117-1124, 1995.
5. W.T. Webb and R. Steele, "Variable Rate QAM for Mobile Radio", *IEEE Trans. on Commun.*, Vol. COM-43, pp. 2223–2230, 1995.
6. A.J. Goldsmith and S.G. Chua, "Variable-Rate Variable-Power M-QAM for Fading Channels", *IEEE Trans. Commun.*, Vol. COM-45, pp. 1218–1230, 1997.

7. H. Matsuoka, S. Sampei, N. Morinaga and Y. Kamio, "Adaptive Modulation System with Variable Coding Rate Concatenated Code for High Quality Multi-Media Communication Systems", in *Proc. IEEE Veh. Technol. Conf. VTC '96*, Atlanta, GA, April 1996, pp. 487–491. Full paper published in the *IEICE Trans. Commun.*, Vol. E79-B, pp. 328–334, 1996.
8. A. Goldsmith, "Variable-Rate Coded M-QAM for Fading Channels", in *Proc. Communication Theory Mini-Conference (CTMC-III) in conjunction with IEEE Global Commun. Conf. GLOBECOM '94*, San Fransisco, CA, November 1994, pp. 186–190.
9. A. Goldsmith and P. Varaiya, "Capacity of Fading Channels with Channel Side Information", *IEEE Trans. on Information Theory*, Vol. IT-43, pp. 1896–1992, 1997.
10. J. M. Torrance and L. Hanzo, "Upper Bound Performance of Adaptive Modulation in a Slow Rayleigh Fading Channel", *Electron. Lett.*, Vol. 32, pp. 718–719, 1996.
11. I. S. Gradshteyn and I. M. Ryzhik, *Table of Integrals, Series, and Products*, Academic Press: San Diego, CA, fifth edn., 1994.
12. H. Suzuki, "A Statistical Model for Urban Multipath Propagation", *IEEE Trans. on Commun.*, Vol. COM-25, pp. 673–680, 1977.
13. A.U. Sheikh, M. Handforth and M. Abdi, "Indoor Mobile Radio Channel at 946 MHz: Measurements and Modeling", in *Proc. IEEE Veh. Technol. Conf. VTC '93*, Secaucus, NJ, May 1993, pp. 73–76.
14. M.-S. Alouini and A. Goldsmith, "Capacity of Rayleigh Fading Channels under Different Adaptive Transmission and Diversity Techniques", *IEEE Trans. Veh. Technol.*, to appear.
15. W.C.Y. Lee, "Estimate of Channel Capacity in Rayleigh Fading Environment", *IEEE Trans. Veh. Technol.*, Vol. VT-39, pp. 187–190, 1990.
16. C.G. Günther, "Comment on 'Estimate of Channel Capacity in Rayleigh Fading Environment' ", *IEEE Trans. Veh. Technol.*, Vol. VT-45, pp. 401–403, 1996.
17. R.J. McEliece and W.E. Stark, "Channels with Block Interference", *IEEE Trans. on Information Theory*, Vol. IT-30, pp. 44–53, 1984.
18. L. Ozarow, S. Shamai and A. Wyner, "Information Theoretic Considerations for Cellular Mobile Radio", *IEEE Trans. on Veh. Technol.*, Vol. VT-43, pp. 359–378, 1994.
19. T. Ericson, "A Gaussian Channel with Slow Fading", *IEEE Trans. Inform. Theory*, Vol. IT-16, pp. 353–355, 1970.
20. Y.-D. Yao and A.U.H. Sheikh, "Evaluation of Channel Capacity in a Generalized Fading Channel", in *Proc. IEEE Veh. Technol. Conf. VTC '93*, Secaucus, NJ, May 1993, pp. 134–137.
21. R. Buz, "Information Theoretic Limits on Communication over Multipath Fading Channels", in *Proc. IEEE Int. Symposium Inform. Theory ISIT '95*, Whistler, BC, Canada, September 1995, p. 151.
22. W.T. Webb and L. Hanzo, *Modern Quadrature Amplitude Modulation*, IEEE Press: New York, 1994.
23. J.G. Proakis, *Digital Communications*, McGraw-Hill, New York, NY, second edn., 1989.
24. G.D. Forney Jr., R.G. Gallager, G.R. Lang, F.M. Longstaff and S.U. Qureshi, "Efficient Modulation for Band-Limited Channels", *IEEE J. Select. Areas Commun.*, Vol. SAC-2, pp. 632–646, 1984.
25. T. Eng and L.B. Milstein, "Coherent DS-CDMA Performance in Nakagami Multipath Fading", *IEEE Trans. Commun.*, Vol. COM-43, pp. 1134–1143, 1995.
26. J.M. Torrance and L. Hanzo, "Optimisation of Switching Levels for Adaptive Modulation in a Slow Rayleigh Fading Channel", *Electron. Lett.*, Vol. 32, pp. 1167–1169, 1996.
27. D. Goeckel, "Robust Adaptive Coded Modulation for Time-Varying Channels with Delayed Feedback", in *Proc. Thirty-Fifth Annual Allerton Conf. on Communication, Control, and Computing*, September 1997, pp. 370–379.
28. W.C. Jakes, *Microwave Mobile Communication*, IEEE Press: Piscataway, NJ, second edn., 1994.
29. N.M. Temme, *Special Functions – An Introduction to the Classical Functions of Mathematical Physics*, John Wiley & Sons: New York, NY, 1996.

Mohamed-Slim Alouini was born in Tunis, Tunisia. He received the "Diplôme d'Ingénieur" degree from the Ecole Nationale Supérieure des Télécommunications (TELECOM Paris), Paris, France, and the "Diplôme d'Etudes Approfondies (D.E.A.)" degree in Electronics from the University of Pierre & Marie Curie (Paris VI), Paris, France, both in 1993. He received the M.S.E.E. degree from the Georgia Institute of Technology (Georgia Tech), Atlanta, GA, U.S.A., in 1995, and the Ph.D. degree in electrical engineering from the California Institute of Technology (Caltech), Pasadena, CA, U.S.A., in 1998.

While completing his D.E.A. thesis, he worked with the optical submarine systems research group of the French national center of telecommunications (CNET-Paris B), on the development of future transatlantic optical links. While at Georgia Tech, he conducted research in the area of K_a-band satellite channel characterization and modeling. From June 1998 to August 1998, he was a Post-Doctoral Fellow with the Communications group at Caltech carrying out research on adaptive modulation techniques and on CDMA communications. He joined the department of Electrical and Computer Engineering of the University of Minnesota, Minneapolis, in September 1998, where his current research interests include statistical modeling of multipath fading channels, adaptive modulation techniques, diversity systems, and digital communication over fading channels.

He is a recipient of a National Semiconductor Graduate Fellowship Award. He is a member of the IEEE Communications and Vehicular Technology Societies.

Andrea J. Goldsmith received the B.S., M.S., and Ph.D. degrees in electrical engineering from U.C. Berkeley in 1986, 1991, and 1994, respectively.

From 1986–1990 she was affiliated with Maxim Technologies, where she worked on packet radio and satellite communication systems, and from 1991–1992 she was affiliated with AT&T Bell Laboratories, where she worked on microcell modeling and channel estimation. She was an assistant professor of Electrical Engineering at the California Institute of Technology

from 1994–1998, and is currently an assistant professor of Electrical Engineering at Stanford University. Her research includes work in capacity of wireless channels, wireless communication theory, adaptive modulation and coding, joint source and channel coding, and resource allocation in cellular systems.

Dr. Goldsmith is a recipient of the National Science Foundation CAREER Development Award, ONR Young Investigator Award, two National Semiconductor Faculty Development Awards, an IBM Graduate Fellowship, and the David Griep Memorial Prize from U.C. Berkeley. She is an editor for the IEEE Transactions on Communications and the IEEE Personal Communications Magazine.